A Linearly Tapered Box Model of the Cochlea

Guangjian Ni, [1] Luyang Sun, [1] and Stephen J Elliott [1]

[1] Institute of Sound and Vibration Research, University of Southampton, Highfield Campus, Southampton SO17 1BJ United Kingdom

Running title: Linearly Tapered cochlear model

Abstract

A box shape with constant area is often used to represent the complex geometry in the cochlea, although variation of the fluid chambers areas is known to be more complicated. This variation is account for here by an "effective area", given by the harmonic mean of upper and lower chamber area from previous measurements. The square root of this effective area varies linearly along the cochleae in the investigated mammalian species. This suggests the use of a linearly tapered box model, in which the fluid chamber width and height are equal, but decrease linearly along its length. The basilar membrane width is assumed to increase linearly along the model. An analytic form of the far-field fluid pressure difference due to basilar membrane motion is derived for this tapered model. The distributions of the passive basilar membrane response are calculated using both the tapered and uniform models and compared with human and mouse measurements. The discrepancy between the models is frequency-dependent and becomes small at low frequencies. The tapered model developed here shows a reasonable fit to experimental measurements, when the cochleae are cadaver or driven at high sound pressure level and provides a convenient way to incorporate cochlear geometrical variations.

Keywords: Cochlear mechanics; fluid coupling; coupled response; tapered model

I. INTRODUCTION

The cochlea is a sensory organ of the hearing system responsible for converting sound-induced motion into electrochemical impulses for perception. Although the cochlea has a coiled structure, e.g. Viergever (1978), Loh (1983), Steele and Zais (1985), the fluid chambers are often modelled using a straight and uniform box model (Ranke, 1950; Lesser and Berkley, 1972; Siebert, 1974; Sondhi, 1978; de Boer, 1996; Vetesník and Nobili, 2006; Elliott *et al*., 2011, 2013). Although the box shape is an overly simplified representation of the real cochlear geometry, the coupled[1] basilar membrane, BM, response to tones, especially the frequency-position tonotopy relation, can still be reproduced reasonably well (de Boer, 1996). The assumption that the box model is rectangular may appear to be physically unrealistic, however, de Boer (1991) has shown that similar results for the three-dimensional, 3D, fluid coupling are obtained if the cross-section is assumed circular. This reflects the fact that the far-field, plane wave, component of the fluid pressure depends mainly on the cross-sectional area of the chambers rather than their shape. If the uniform box model represents a first approximation to the cochlear geometry, for the calculation of the fluid coupling (Steele and Taber, 1981; de Boer, 1996; Elliott *et al.*, 2011; Ni and Elliott, 2015), a sensible second approximation would thus appear to be a linearly tapered box model, as shown in Fig. 1.

Puria and Allen (1991) include exponential scalae tapering in a transmission line model of the cochlea and find it has a significant effect on the cochlear input impedance. Similarly, Shera and Zweig (1991) also consider the effects of tapering and point out that the width of the basilar membrane and the scalae area taper in opposite directions, enabling a slow variation of wavelength near the stapes, which provides an efficient energy transfer between the middle and inner ears at low frequencies. The differences between the linearly tapered box model and the transmission line models previously used are that the cross-sectional area varies in a

[1] The term "coupled" in this paper refers to fluid-structure coupling.

linear way in this paper rather than exponentially from the base and the basilar membrane width varies linearly as well. Although not shown in this paper, the cochlear input impedance of the linearly tapered model increases with frequency and is greater than that calculated using a uniform model, which is consistent with previous prediction using the transmission line models. More recently, Kim *et al*. (2011) develop a finite element model of the cochlea for analyzing the mechanism of bone conduction hearing, in which the BM and cochlear partition width, together with the height of the fluid chambers vary approximately linearly along the straight box model.

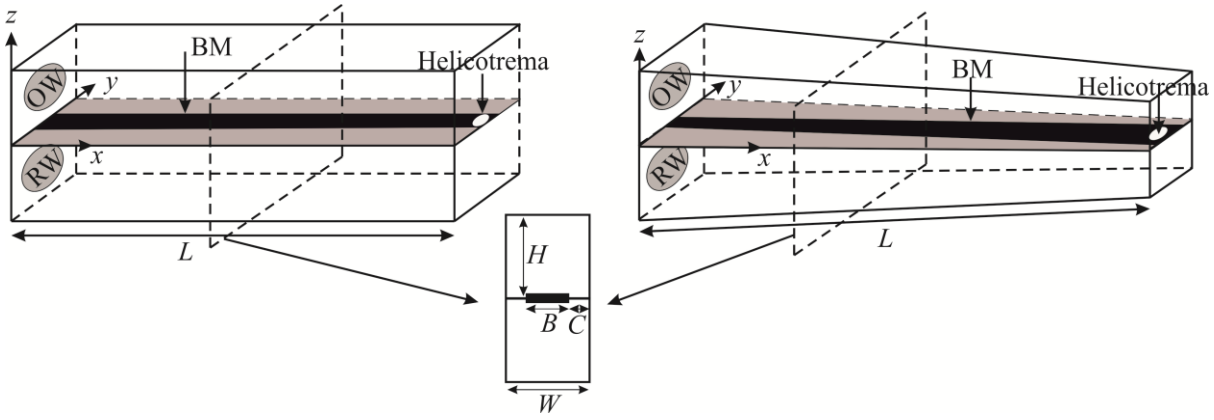

FIG. 1. Sketches of a uniform box model (left), in which the fluid chamber height, *H*, width, *W*, and the basilar membrane width, *B*, are constant, a linearly tapered box model (right), in which the cross-sectional area decreases whereas the basilar membrane width increases from the base to the apex, and a cross-section (middle). In both models, the lower and upper chambers are assumed to be identical and exchange fluid via the helicotrema provides a zero pressure difference at $x=L$.

There are many methods to solve the cochlear box models, for example the Wentzel–Kramers–Brillouin, WKB, method (Zweig *et al*., 1976; Steele and Taber, 1979a, 1979b; Wang *et al*., 2016), the finite element method (Kim *et al.*, 2011; Elliott *et al.*, 2013; Ni and Elliott, 2015), and the finite difference method (Neely, 1985). Different methods have their own assumptions and limits, such as only one wave with slow variation travelling in one direction in the WKB method, or at least six elements within the shortest wavelength interested in the finite element/difference methods (Fahy and Gardonio, 2007). The method

used in this paper is an extension of Elliott *et al*. (2011), which employs a matrix formulation for solving the fluid coupling and the cochlear response, as described below. One advantage of this approach is to provide a closed-form solution to the far-field fluid coupling, which depends on the cochlear geometry, that can be used in analyzing complicated cochlear structure at a low computational cost compared with the finite element solution (Ni *et al.*, 2011), for example.

The fundamental mechanics of the passive, postmortem, cochlea can be thought as an interaction between the fluid inertia along the fluid chambers and the dynamic behavior of the cochlear partition that separates them (de Boer, 1996). The fluid pressure due to a moving element of the basilar membrane can be decomposed into two components (Steele and Taber, 1979a; Elliott *et al*., 2011). That due to the plane wave component of the pressure is called the far-field (or long-wavelength) component, and that due to the pressure variations close to the basilar membrane is called the near-field (or short-wavelength) component. The far-field component, which is associated with wavelengths that are large compared with the size of the fluid chambers, plays an important role in the cochlear travelling wave propagation. The near-field component is associated with short wavelength and affects the cochlear partition motion by introducing a fluid added mass on the basilar membrane (Neely, 1985; de La Rochefoucauld and Olson, 2007) and an inertial term to the local longitudinal coupling along the cochlea (Steele and Taber, 1981; Parthasarathi *et al.*, 2000; Elliott *et al.*, 2011). The far-field pressure mainly depends on the geometric features, such as cross-sectional area and coiling of the cochlear fluid chambers (Manoussaki and Chadwick, 2000; Cai *et al.*, 2005; Ni *et al.*, 2011), whereas the near-field pressure is not substantially affected by the fluid chamber geometry and could be calculated from the local arrangement of the basilar membrane, using various methods (Ni and Elliott, 2015).

The areas of the upper fluid chamber, which includes the scala media, SM, and scala vestibuli, SV, and of the lower fluid chamber, which includes the scala tympani, ST, vary along the length of the cochlea, x, as $A_1(x)$ and $A_2(x)$, respectively. The cochlear fluid is assumed to be incompressible and inviscid, since the effects of fluid viscosity and compressibility are generally considered to be not as important as the fluid inertia for the cochlear macromechanics (Viergever, 1980; Neely, 1985), although viscosity is shown to play a key role in cochlear power flow (Wang, *et al*., 2016). The following derivations are based on these assumptions but are not limit to inviscid fluid. The far-field component of the pressure can be determined by combining the conservation of mass and momentum equations. Assuming that the fluid longitudinal velocity in a single chamber, here the upper fluid chamber is chosen for illustration, averaged across its cross-sectional area is $\bar{u}(x)$, and that the radial basilar membrane velocity, averaged across the width of the chamber, is $\bar{v}(x)$, which is positive towards the scala vestibuli (upwards). The continuity equation for the upper chamber can then be written as

$$\frac{\partial}{\partial x}[A(x)\bar{u}(x)] = W(x)\bar{v}(x), \tag{1}$$

where $A(x)$ and $W(x)$ are the chamber cross-sectional area and width. This is equivalent to the equation used by Peterson and Bogert (1950).

The momentum equation can also be written in terms of the complex pressure, $\bar{p}(x)$, averaged across the cross-sectional area, as

$$\frac{\partial \bar{p}(x)}{\partial x} = -i\omega\rho\bar{u}(x), \tag{2}$$

where ρ is the density of the cochlear fluid, ω is angular frequency and $i = \sqrt{-1}$.

Substituting $\bar{u}(x)$ in equation (2) into equation (1) gives an expression for $\bar{p}(x)$ in terms of $\bar{v}(x)$ as

$$\frac{\partial}{\partial x}\left[A(x)\frac{\partial \bar{p}(x)}{\partial x}\right] = -i\omega\rho W(x)\bar{v}(x), \tag{3}$$

which is an incompressible form of Webster's horn equation, as described by Fletcher and Rossing (2008), for example. Shera *et al*. (2004) derive a similar expression, equation (A1) in Shera *et al*. (2004) Appendix A, for the far-field, long-wavelength, fluid coupling in a tapered cochlear model with a constant BM width.

Geometrical features, such as the cross-sectional area of the fluid chambers, are crucial for quantitative modelling of the cochlea. Thorne *et al.* (1999) derived cochlear fluid space dimensions for different species from reconstructions of three-dimensional magnetic resonance microscopy including areas of the SV, SM and ST, which are used in this study for constructing a tapered model of the cochlea. The mouse cochlea geometry, however, is taken from a more recent work by Rau *et al.* (2012) to cover a larger number of spatial positions.

In calculating the coupled response of the cochlea, we focus on the passive case, whose normalized distribution is similar to those measured at high sound pressure levels, SPLs, excitations, e.g. over 80 dB SPL, because of the simplicity of the micromechanical model in this case. The structure of the paper is that Section II reviews the geometric variation of the fluid chambers along the length of different cochleae. In Section III, expressions for the far-field and near-field fluid coupling of tapered fluid chambers are derived. In Section IV, the fluid coupling in the tapered and uniform model of the human cochlea is calculated, as well as the fluid added mass distribution in the cochleae of five different species. The uniform model here takes mean geometrical values over the length of the linearly tapered model. In Section V, the coupled response of the cochlea is calculated using the linearly tapered and uniform models of the human and mouse cochleae and compared with experimental measurements.

II. GEOMETRICAL VARIATION IN DIFFERENT SPECIES

There are several sources of information about the variation in the physical dimensions of the fluid chambers, along the length of the cochlea in different species, among which the

database of Salt's lab[2] provides the most comprehensive set. The measured geometrical variations in the fluid chambers and cochlear partition in a number of species are used here to calculate the cross-sectional area, the basilar membrane width, and derived variables, such as the effective area.

A. Variation of the fluid chambers

One parameter for the far-field fluid coupling is the effective area, as described in detail in Section III, which is calculated based on the upper and lower fluid chamber areas, $A_1(x)$ and $A_2(x)$, respectively. Since the fluid coupling is not sensitive to the shape of the fluid chamber cross-sectional area (de Boer, 1991), it is mathematically convenient to assume that the cross-section is square. So that the equivalent fluid chamber width and height, W_e and H_e, are equal to square root of the effective area, $A_e(x)$, as

$$H_e(x) = W_e(x) = \sqrt{A_e(x)}, \tag{4}$$

where the effective area is written in the form of the harmonic mean as (Peterson and Bogert, 1950; Zwislocki, 1953)

$$A_e(x) = \frac{2A_1(x)A_2(x)}{A_1(x)+A_2(x)}. \tag{5}$$

Variations of the upper and lower fluid chamber areas and the calculated effective area in different species are shown in Fig. 2 with respect to a non-dimensional longitudinal position, i.e. longitudinal position, x, over the cochlear length, L. The variation of the lower fluid chamber area is seen to be steeper than that of the upper fluid chamber among all the selected species, especially at the basal end. All measured geometrical data, to our knowledge, does not cover the entire length of the cochleae, which implies extrapolation is necessary for modelling purpose.

[2] Alec Salt's lab: http://oto2.wustl.edu/cochlea/

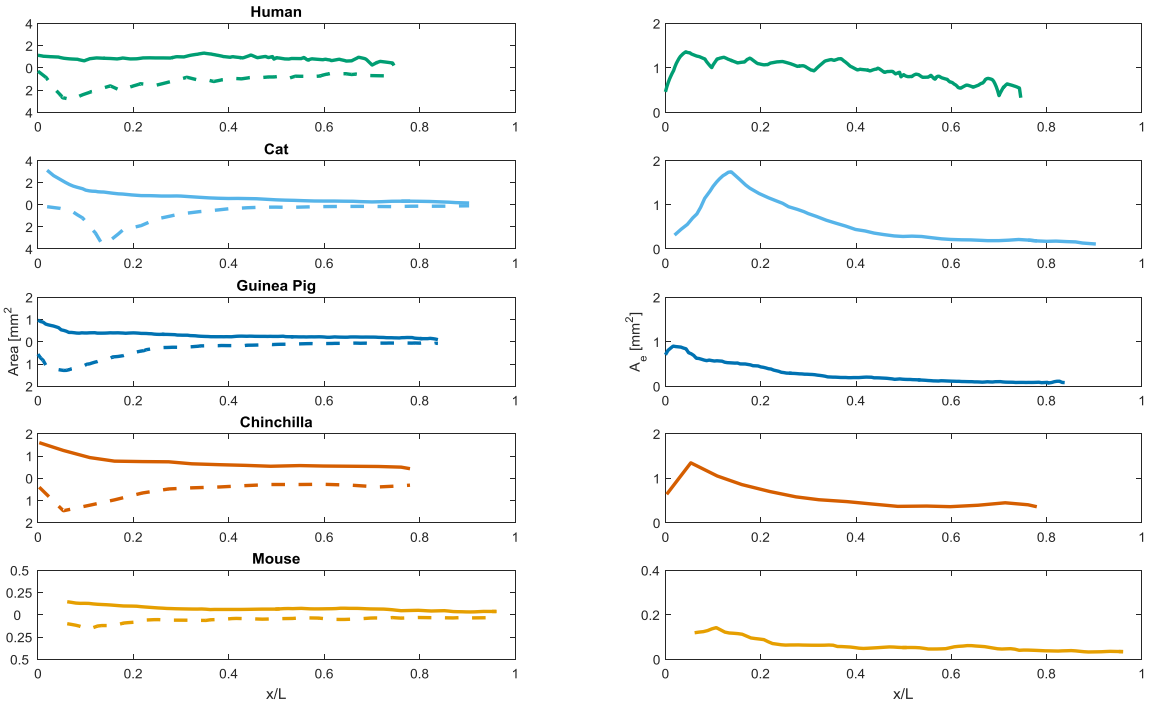

FIG. 2. (color online) Variation of the fluid chamber areas, A_1 (solid line) and A_2 (dashed line) in five different species (left panel) and calculated effective area, A_e, using equation (5) (right panel). All parameters are plotted against a length scale normalized by the physical length of the cochleae.

Figure 3 shows the variation of the fluid chamber equivalent height, H_e, and its linearized approximation using the least squares method. It is interesting to see that although the area variations in the two fluid chambers are different among the different species, the square root of the effective area can be reasonably well approximated by a linear fit. The linear fit overestimates the true values by about 11% near the base where the anatomical geometry is known to be more complicated and many other factors such aqueducts, round window dynamics etc., may play a more significant role, so that we assume that this overestimate of the effective area can be ignored when we compare model predictions with measurements later. There are other approximations, such as exponential, e.g. Puria and Allen (1991), or polynomial functions, which may provide a better fit to the measured data. In this paper, however, a linearly tapered model is used, as motivated by the results shown in Fig. 3 and also as the simplest development of a uniform box model. It should also be noted that this model is reasonably consistent with an exponential tapering, proving the tapering is not too great, since

$$\text{if } A_e(x) = A_0 e^{-\alpha x}, \text{ then } \sqrt{A_e(x)} = \sqrt{A_0} e^{-\alpha x/2} \approx \sqrt{A_0}(1 - \alpha x/2), \qquad (6)(7)$$

provided $(\alpha x/2)^2 \ll 1$.

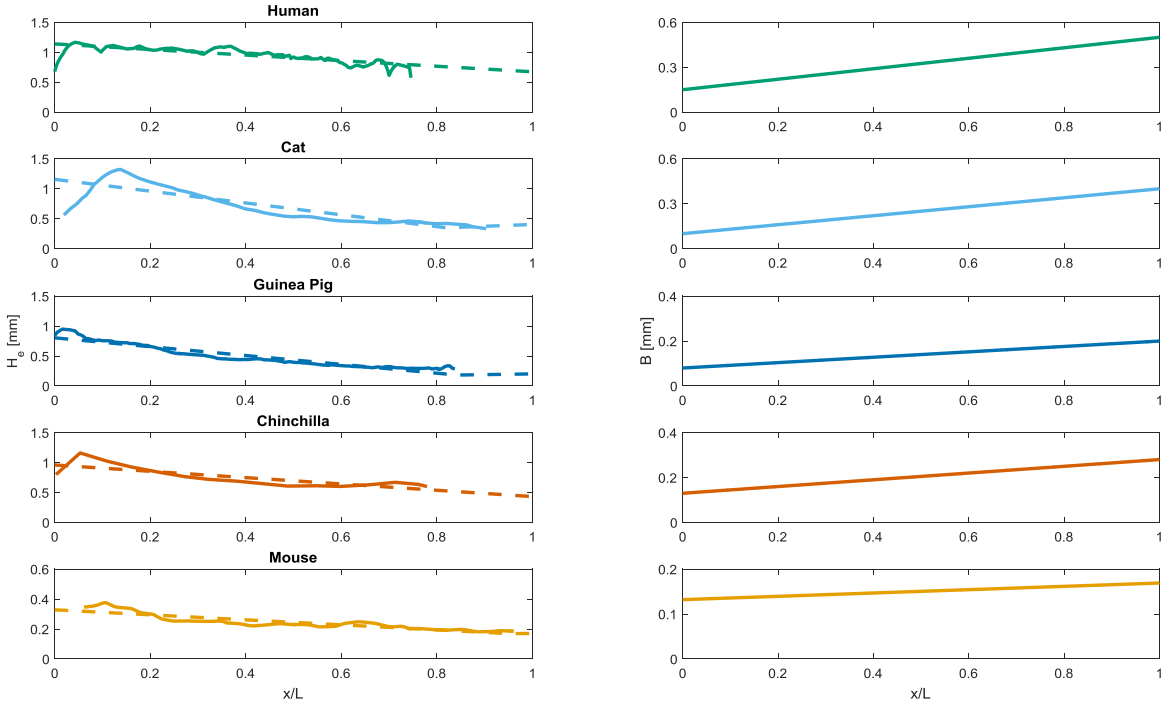

FIG. 3. (color online) Variation of the equivalent height (solid line), H_e, and its linear approximations (dashed line) (left panel), and the assumed variation of the BM width, B, in different species (right panel). The BM width are taken from the literature for human (Wever, 1949), for cat (Cabezudo, 1978), for guinea pig (Fernández, 1952), for chinchilla (Dallos, 1970), and for mouse (Keiler and Richter, 2001). All variables are plotted against a length scale normalized by the physical length of the cochleae.

Values for those linearized fluid chamber equivalent height are listed in Table I, in which a constraint has been imposed that the fluid chamber equivalent width (equal to the equivalent height, as defined in equation (4)) should be no less than the basilar membrane width. The correlation coefficient, r, for the least squares fit, as also shown in Table I, is calculated using *corr* command in MATLAB™ (R2015b).

B. Variation of the basilar membrane width

The basilar membrane is assumed to take up the middle part of the cochlear partition that separates the two fluid chambers, as shown in Fig. 1. The variation of the basilar membrane width, $B(x)$, from the base to the apex was measured by Fernández (1952) for the guinea pig and human, and measured or assumed by others for other species, as shown in Table I and

Fig. 3. Previous observations show that the variation of the basilar membrane width is approximately linear along the length of the cochleae and can be given by

$$B_l(x) = B_B + \frac{B_A - B_B}{L}x, \tag{8}$$

where B_A and B_B stand for the basilar membrane width at the apex and base, respectively, and L is the length of the cochleae.

TABLE I. Parameters of the tapered box model of the passive cochlea of five different species. Values are from either measurements or models in literatures: (a) Cabezudo (1978), (b) Dallos (1970), (c) Wever (1949), (d) Fernández (1952), (e) Greenwood (1990), (f) Keiler and Richter (2001), and (g) Liberman (1982).

Variable	Symbol	Human	Cat	Guinea pig	Chinchilla	Mouse
Length (mm)	L	35 (e)	25 (g)	18.5 (e)	18.4 (e)	7 (e)
Linearized equivalent height at the base (mm)	H_{lB}	1.14	1.16	0.80	0.96	0.33
Linearized equivalent height at the apex (mm)	H_{lA}	0.67	0.40	0.20	0.43	0.17
BM width at the base (mm)	B_B	0.15 (c)	0.10 (a)	0.08 (d)	0.13 (b)	0.13 (f)
BM width at the apex (mm)	B_A	0.50 (c)	0.40 (a)	0.20 (d)	0.28 (b)	0.17 (f)
Frequency at the base (kHz)	f_B	20 (e)	60 (g)	44 (e)	20 (e)	105 (e)
Characteristic length for frequency variation (mm)	l	7	5.1	3.8	3.8	1.5
Length ratio	L/l	5	5	4.7	4.8	4.6
Linear correlation coefficient	r	0.82	0.84	0.95	0.81	0.89

C. Distribution of the characteristic frequency

The mechanism underlying the cochlear frequency-position mapping characteristic is believed to be similar in most mammals (Robles and Ruggero, 2001). There is, however, a wide range of physical dimensions of the cochlea in different mammals, resulting in difference in perceptible hearing frequency range. Greenwood (1990) develops a function that maps the characteristic frequency, CF, onto locations along the length of the cochlea, as

$$\mathrm{CF} = f_h\left(10^{\alpha(L-x)/L} - f_l\right), \tag{9}$$

where x stands for distance away from the base, f_h is a constant controlling the high-frequency limit, α is a constant that controls the slope of the frequency map, L is again the length of the cochlea, and f_l is a constant controlling low-frequency limit. Here we ignore the factor f_l above, and simplify the characteristic frequency function to

$$\mathrm{CF} = f_{\mathrm{B}} e^{-x/l}, \tag{10}$$

where f_{B} is the characteristic frequency at the base, equal to $f_h 10^{\alpha}$, and l is the characteristic length, equal to $x/\ln 10^{\alpha x/L}$.

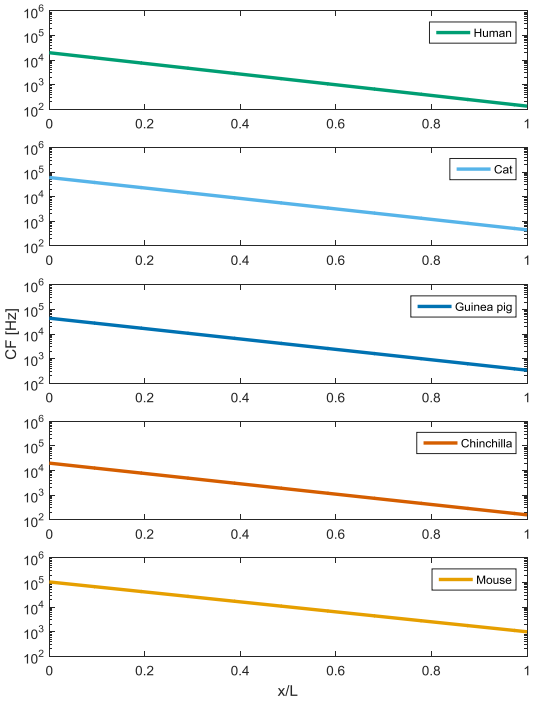

FIG. 4. (color online) Distributions of the characteristic frequency along the cochlea in five species. The position along the cochlea, from the base, is normalized by the physical length of the cochleae.

Figure 4 shows the spatial variation of characteristic frequency for the five species, based on parameters listed in Table I. It is interesting to see that although different species have different characteristic frequency distributions along their length, they are almost parallel with each other if they are plotted against position normalized by the length of the cochlea. The ratio of the cochlear length, L, to the characteristic decay length, l, is thus approximately constant, and has a value of about 5, as shown in Table I, among different species, and so the frequency ranges of the cochleae in different species are always about 7 octaves, as shown in Fig. 4.

III. FLUID COUPLING IN A NON-UNIFORM COCHLEA

A. Far-field component

The fluid coupling and the BM velocity can be analyzed using a single longitudinal variable, *x*, along the cochleae (Steele and Taber, 1979b; de Boer, 1984; Elliott *et al*., 2011), which reduce the three-dimensional model to a uni-dimensional while still accounting for its radial, *y*, and vertical, *z*, characteristics. The averaged BM radial velocity, $\bar{v}(x)$, in equation (3), can thus be defined as

$$\bar{v}(x) = \frac{v(x)}{W(x)} \int_0^{W(x)} \psi(y) dy, \tag{11}$$

where $\psi(y)$ is the BM velocity, $v(x)$, radial profile and generally assumed as half-sinusoidal and normalized over the BM width, *B*, as $\psi(y) = \sqrt{2W/B}\sin(\pi y/B)$ (Steele and Taber, 1979b).

In the far-field limit, the pressure is uniform over the BM, so that the modal pressure in the upper fluid chamber, $p_1(x)$, can be given as

$$p_1(x) = \frac{\bar{p}(x)}{W(x)} \int_0^{W(x)} \psi(y) dy. \tag{12}$$

Substituting equations (11) and (12) into equation (3) gives the far-field fluid coupling in the upper chamber, as

$$\frac{\partial}{\partial x}\left[A_1(x)\frac{\partial}{\partial x}\left(p_1(x)\sqrt{\frac{W(x)}{B(x)}}\right)\right] = -\frac{8i\omega\rho}{\pi^2} v(x)\sqrt{W(x)B(x)}. \tag{13}$$

In general, the far-field fluid coupling in the lower fluid chamber is similarly related to the modal BM velocity as

$$\frac{\partial}{\partial x}\left[A_2(x)\frac{\partial}{\partial x}\left(p_2(x)\sqrt{\frac{W(x)}{B(x)}}\right)\right] = \frac{8i\omega\rho}{\pi^2} v(x)\sqrt{W(x)B(x)}. \tag{14}$$

The integral of the right-hand side of equations (13) and (14) with respect to *x* is thus equal to both of the expressions below

$$\frac{8i\omega\rho}{\pi^2}\int_0^x v(x')\sqrt{W(x')B(x')}dx' = A_2(x)\frac{\partial}{\partial x}\left(p_2(x)\sqrt{\frac{W(x)}{B(x)}}\right) = -A_1(x)\frac{\partial}{\partial x}\left(p_1(x)\sqrt{\frac{W(x)}{B(x)}}\right), \tag{15}$$

where x' is dummy integration variable. The pressure gradients in the two chambers are related by

$$\frac{\partial}{\partial x}\left(p_2(x)\sqrt{\frac{W(x)}{B(x)}}\right) = -\frac{A_1(x)}{A_2(x)}\frac{\partial}{\partial x}\left(p_1(x)\sqrt{\frac{W(x)}{B(x)}}\right). \quad (16)$$

We can relate the far-field component of the modal pressure difference, $p_F(x)= p_1(x)-p_2(x)$, to the modal BM velocity, $v(x)$, via the effective area $A_e(x)$ in the expression as

$$\frac{\partial}{\partial x}\left[A_e(x)\frac{\partial}{\partial x}\left(p_F(x)\sqrt{\frac{W(x)}{B(x)}}\right)\right] = -\frac{16i\omega\rho}{\pi^2}v(x)\sqrt{W(x)B(x)}. \quad (17)$$

An analytic solution to the pressure difference can be obtained for excitation of a single BM element, having a velocity of v_0 from x_0–Δ to x_0 and zero elsewhere. The boundary condition that $p_F(x)$ is zero at $x = L$ and the fact that Δ is small compared with L can then be used to integrate equation (17) twice to give

$$p_F(x)|_{0<x<x_0-\Delta} = -\frac{16i\omega\rho\Delta^2 v_0}{\pi^2}\sqrt{\frac{W(x_0)B(x_0)B(x)}{W(x)}}\int_{x_0}^{L}\frac{1}{A_e(x\prime)}dx', \quad (18)$$

$$p_F(x)|_{x_0<x<L} = -\frac{16i\omega\rho\Delta^2 v_0}{\pi^2}\sqrt{\frac{W(x_0)B(x_0)B(x)}{W(x)}}\int_{x}^{L}\frac{1}{A_e(x\prime)}dx', \quad (19)$$

where x' is again dummy integration variable. It is computationally convenient to divide a continuous system into a number of discrete elements, which may be taken as an accurate representation of the continuous system if there are at least six elements within the shortest wavelength present, which is a condition commonly used in finite element analysis (Fahy and Gardonio, 2007). If the areas of the fluid chambers in the cochlear models are divided up into N discrete sections, as for the BM, the integrals in equations (18) and (19) can be approximated by summations to give the pressure at the n-th element as

$$p_F(n)|_{0<n<n_0-1} = -\frac{16i\omega\rho\Delta^2 v_0}{\pi^2}\sqrt{\frac{W(n_0)B(n_0)B(n)}{W(n)}}\sum_{n'=n_0}^{N}\frac{1}{A_e(n\prime)}, \quad (20)$$

$$p_F(n)|_{n_0<n<N} = -\frac{16i\omega\rho\Delta^2 v_0}{\pi^2}\sqrt{\frac{W(n_0)B(n_0)B(n)}{W(n)}}\sum_{n'=n}^{N}\frac{1}{A_e(n\prime)}, \quad (21)$$

where $n_0 = x_0/\Delta$.

B. Near-field component

It is significant that the near-field pressure is greatest in the immediate vicinity of the vibrating BM and is small on the further surfaces of the fluid chamber. The near-field pressure is thus relatively independent of the shape of the fluid chambers. Elliott *et al*. (2011) show that there are no many variations over the range $B/W = 0.11$ to $B/W = 0.99$, as displayed in the tapered model, which suggests that the shape of these near-field components is relatively independent of B/W.

Apart from the physical mass per unit area of the BM, fluid added loading, due to the fluid inertia, will provide some additional mass. In a one-dimensional, 1D, model, in which only the far-field component is considered, of the cochlea, there is an effective additional thickness of the BM due to the fluid loading, that can be calculated using the wavenumber analysis of fluid coupling (Steele and Taber, 1979b; Elliott *et al*., 2011). When take equation (4) into account, this effective thickness of the BM can be given as

$$T_f(x) = \frac{8B(x)}{3\pi^2} + \sum_{n=1}^{\infty} \frac{4B(x)}{n\pi^3} \coth(n\pi) \left\{ \frac{\cos[n\pi C(x)/W(x)] + \cos\left[n\pi\left(C(x)+B(x)\right)/W(x)\right]}{1-n^2B^2(x)/W^2(x)} \right\}^2, \quad (22)$$

where $C(x)$ is the distance from one side of the cochlear partition to the corresponding edge of the BM, as shown in Fig. 1.

The total BM mass per unit area is thus given by

$$m_0(x) = \rho\left[T_t + T_f(x)\right], \quad (23)$$

where T_t is the sum of the physical thickness due to the organ of Corti, OC, T_{OC}, and the BM, T_{BM}, and T_f is the effective thickness due to the fluid loading.

The physical thickness of the organ of Corti and the BM can be given by

$$T_{\mathrm{OC}} = \frac{A_{\mathrm{OC}}}{B}, T_{\mathrm{BM}} = \frac{A_{\mathrm{BM}}}{B}, \quad (24)(25)$$

where A_{OC} is the average area of the organ of Corti and A_{BM} is the average area of the basilar membrane.

The fluid added mass, due to the near-field component, on the BM along its length are calculated using equation (22), as shown in Fig. 5, for five different species. Since the sum of the physical thickness due to the organ of Corti and the BM, T_t, is significantly less than the effective thickness due to the fluid loading, T_f, the variation of T_t along the cochlea is not shown here and an average value is used in the models.

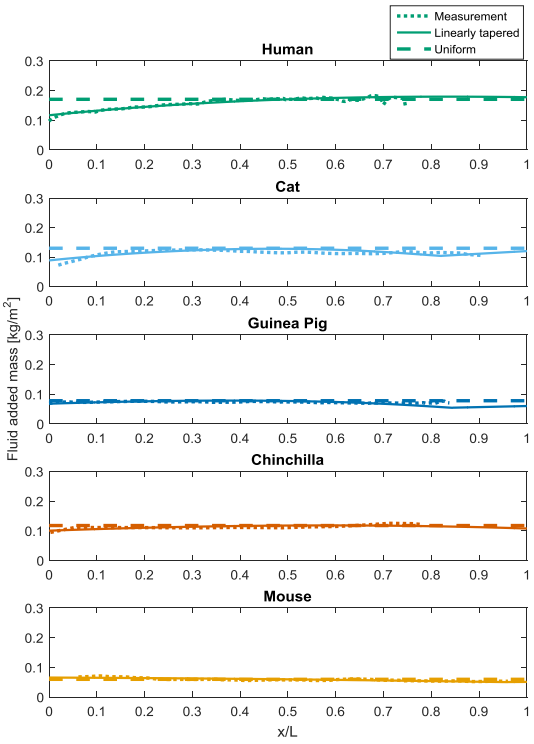

FIG. 5. (color online) Distribution of the fluid added mass for the linearly tapered models (solid lines), the uniform models (dashed lines) and those calculated using measured geometry (dotted lines). All variables are plotted against a length scale normalized by the physical length of the cochleae.

IV. FLUID COUPLING IN A TAPERED BOX MODEL

The distribution of the modal pressure differences with both far- and near-field components, due to excitation by a single element of the BM at 5 mm, 15 mm and 25 mm away from the base are calculated for both the uniform and tapered box models for the human cochlea, as shown in Fig. 6. The far- and near-field components have also been calculated separately for the tapered and uniform cases, in which equations (20) and (21) are used for the far-field

component and the wavenumber approach (Steele and Taber, 1979b) is used for the near-field component. In the uniform case, the BM width, B, and fluid chamber width, W, are assumed to be the mean value of the linear fits, B_l and W_l, which equal to 0.32 mm and 0.9 mm, respectively. It can be seen from Fig. 6 that close to the basal region, when a single element of the BM is driven, at 5 mm for example, the pressure difference of the uniform model is greater than that of the tapered case implying higher fluid impedance in the uniform model, which leads to a smaller basilar membrane motion. This is not surprising since the effective area of the tapered model is greater than that of the uniform model in the basal region, as seen in Fig. 3, in which the effective area equal to square of the equivalent height. The curvature in the pressure difference distribution for x greater than x_0 is due to the reduction of the effective area with distance. The near-field component is seen to be insensitive to the tapering, as the difference between the two models is hardly visible.

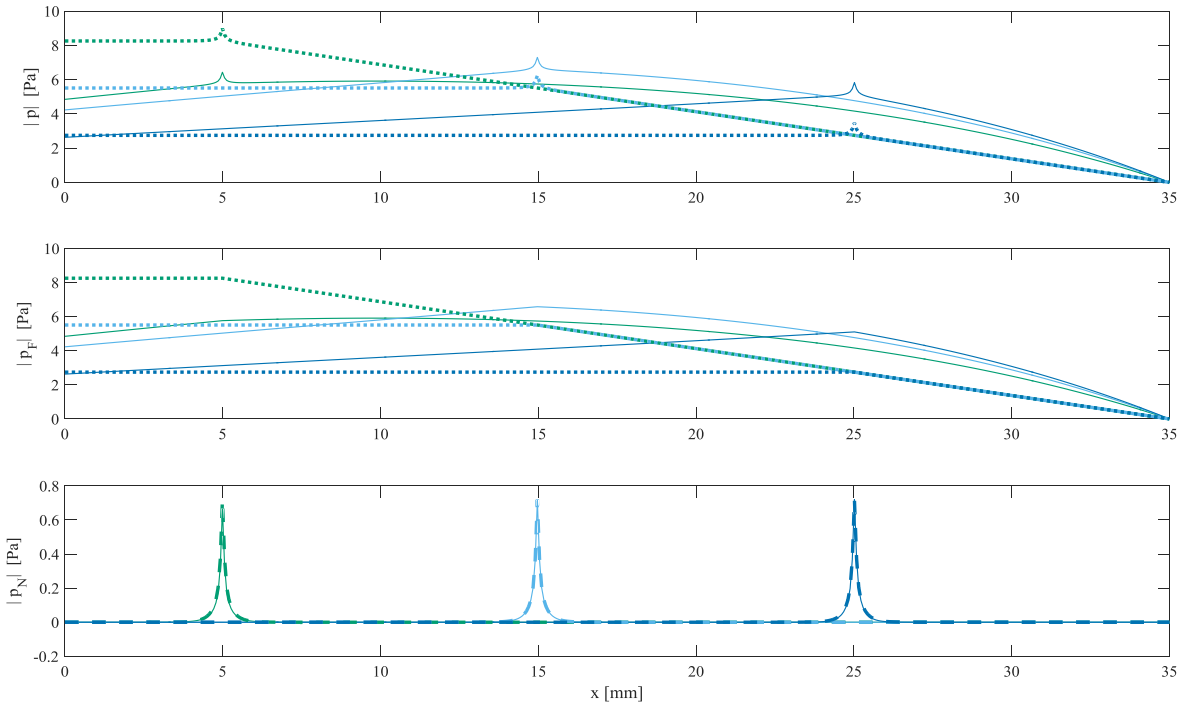

FIG. 6. (color online) The calculated total variation of the modal pressure difference due to both far and near-field components in the tapered (solid lines) and uniform (dashed lines) box model of the human cochlea, when only a single element of the discrete BM at 5 mm, 15 mm and 25 mm is driven sinusoidally with a velocity of 1 mm·s^{-1} at a frequency of 1 kHz, together with the individual far-field, p_F, and near-field, p_N, components.

V. COUPLED RESPONSE IN A TAPERED MODEL OF THE COCHLEA

The coupled behavior of the linear cochlear dynamics can be calculated using a representation of the pressure distribution, driven by the BM movement, and the BM admittance in response to the imposed excitation (Neely, 1985; Elliott *et al*., 2011). The fluid-structure coupling defined here represents a weak coupling between the fluid and structure, the BM, since each domain is separately calculated and then combined to give the coupled response, as illustrated below. This type of discrete expression is generally used for uniform and symmetric box models of the cochlea, using the finite difference method (Steele and Taber, 1979b; de Boer, 1981; Neely, 1981; de Boer and Viergever, 1982).

If the stapes velocity is assumed to be zero, the vector of pressures, $\mathbf{p}$, due to the vector of BM velocities, $\mathbf{v}$, can be written as (Neely, 1981; Elliott *et al.*, 2011)

$$\mathbf{p} = \mathbf{Z}_{\mathrm{FC}}\mathbf{v}, \tag{26}$$

where $\mathbf{Z}_{\mathrm{FC}}$ is a matrix of the fluid coupling impedances and its columns can be obtained by calculating a position-shifted sequence of the pressure distributions, as shown in Fig. 6, normalized by the velocities of each element.

Similarly, the vector of BM velocities can be written as

$$\mathbf{v} = \mathbf{v}_{\mathrm{s}} - \mathbf{Y}_{\mathrm{BM}}\mathbf{p}, \tag{27}$$

where $\mathbf{v}_{\mathrm{s}}$ is a vector that accounts for the stapes velocity and $\mathbf{Y}_{\mathrm{BM}}$ is the BM admittances matrix. $\mathbf{Y}_{\mathrm{BM}}$ will be a diagonal matrix, if the BM reacts only locally. The vector of BM velocities can be given by substituting equation (26) into (27), as

$$\mathbf{v} = [\mathbf{I} + \mathbf{Y}_{\mathrm{BM}}\mathbf{Z}_{\mathrm{FC}}]^{-1}\mathbf{v}_{\mathrm{s}}. \tag{28}$$

The boundary conditions of the tapered and uniform models in this paper are: 1) rigid wall on the external sides of the fluid chambers, 2) the BM is simply-supported at two ends, 3) pressure difference at the helicotrema is zero to account for the fact that the upper and lower chamber exchange fluid there, and 4) excitation is the stapes velocity, $\mathbf{v}_{\mathrm{s}}$.

An advantage of this matrix form is that complicated geometries only need to be analyzed once to determine the elements of $\mathbf{Z}_{\mathrm{FC}}$ and then the coupled responses can be calculated simply using equation (28), for a variety of models, with known or assumed BM dynamics.

The passive BM can be approximated by a series of isolated single-degree-of-freedom systems, whose mechanics at a given position and frequency is given by

$$Y_{\mathrm{BM}}(x,\omega) = -\frac{v(x,\omega)}{p(x,\omega)} = \frac{i\omega}{i\omega r(x) + s(x) - \omega^2 m(x)}, \tag{29}$$

where v is the model BM velocity, p is the model pressure difference, $r(x)$, $s(x)$ and $m(x)$ are damping, stiffness and mass of the BM, per unit area, respectively. The mass, $m(x)$, includes the physical mass due to the organ of Corti and the BM, and the fluid added mass, as given by equation (23). The stiffness is chosen to give the correct natural frequency at each position (meet the frequency-position map of the cochlea), as

$$s(x) = \omega_{\mathrm{n}}^2(x) m(x), \tag{30}$$

where $\omega_{\mathrm{n}}(x)$ is the angular form of the characteristic frequency, given by equation (10), and thus equal to $2\pi f_{\mathrm{B}} e^{-x/l}$. Damping is defined by the quality factor, Q, which is assumed to be constant along the cochlea, so is given by

$$r(x) = \frac{\sqrt{s(x)m(x)}}{Q}. \tag{31}$$

Figure 7 shows a comparison of the calculated BM velocity along the cochlea for the linearly tapered and two uniform models of the human cochlea, at three different excitation frequencies. The two uniform models have parameters that are either those in the middle of the tapered box model, i.e. average parameters, or those at base of the tapered model, as used in the comparisons of Puria and Allen (1991) and Shera and Zweig (1991). It can be seen that the amplitude distributions between the models are similar, except for the magnitude and position of the BM velocity peak change from one model to another. Since the BM admittance of all the models is defined to be identical, it is probably the difference in the fluid added mass, as shown in Fig. 5, that causes the shift in the position of the peak BM velocity.

The fluid added mass of the linearly tapered model is small at the base (high-frequency region) and then increases until slightly greater than that of the uniform models at the apex (low-frequency region). Since the input impedance of the tapered model is greater than that of the uniform models (Puria and Allen, 1991; Shera and Zweig, 1991), then more power is supplied at the stapes of the tapered model, for a constant stapes velocity, than for the uniform box model, and this leads to a greater peak BM velocity. Another effect at low frequencies, however, is that the ratio between the BM width and the fluid chamber width, *B*/*W*, in the linearly tapered model becomes much larger than in the uniform model with averaged parameters, which leads to a decrease of the peak BM velocity.

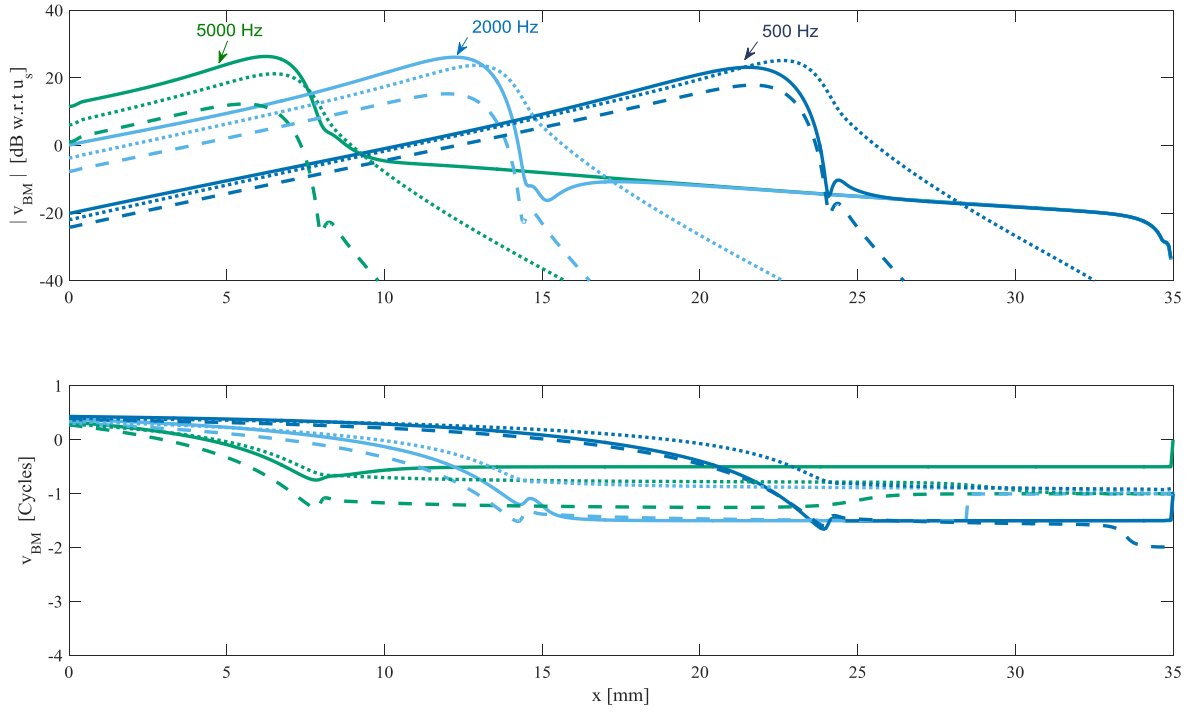

FIG. 7. (color online) The distributions of BM velocity magnitude and phase along the linearly tapered model (solid), uniform model with average parameters (dashed) and uniform model with parameters at the base (dotted) of the human cochlea. The results are normalized with respect to the velocity at the stapes, u_s.

Figure 8 shows the BM frequency response calculated at about 12 mm from the base for the human cochlea in comparison with the BM response measured in a human cadaver by Gundersen *et al.* (1978) and Stenfelt *et al.* (2003). Results are plotted against a non-dimensional variable, $f/\mathrm{BF}(x_0)$ (Zweig, 1976; Shera, 2007), where f is the driving frequencies

and BF(x_0) denotes the best frequency, at which the BM motion is maximum for the level at which the measurement was performed. It can be seen that the human tapered model prediction is similar to those from experiments, although the amplitude has a sharper drop compared with Stenfelt *et al*. (2003). The uniform model predicts an even faster decrease with a peak that is about 10 dB less than the tapered model around the best frequency. The other difference between the two models is that amplitude of the tapered model shows a nearly flat distribution similar to the slow decrease found in the experiments but missing in the uniform model. The roll-off of both the tapered and uniform model is less than that from experimental measurements.

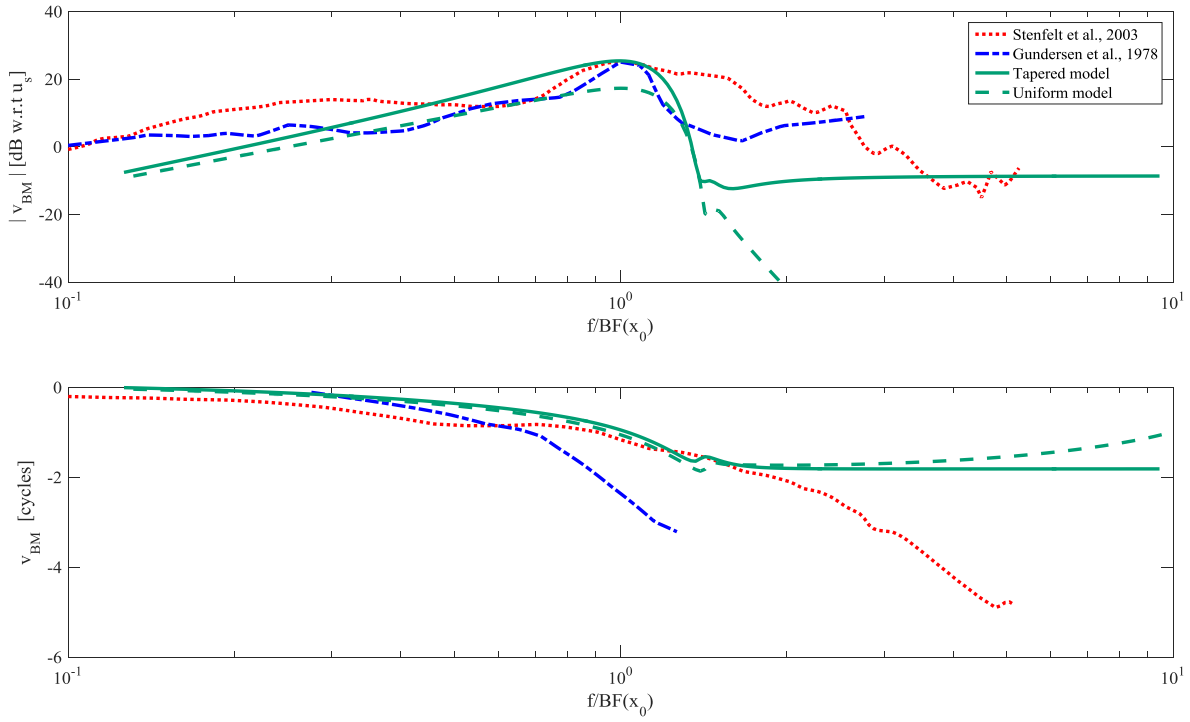

FIG. 8. (color online) The frequency response of the BM velocity magnitude and phase of the linearly tapered and uniform human cochlear models with a Q factor of 2.5, together with experimental measurements (Gundersen *et al.*, 1978; Stenfelt *et al.*, 2003) for the human cadaver. Frequencies are normalized by the best frequency, BF(x_0) ≈ 1.2 kHz, at this level.

Figure 9 shows another comparison between the mouse models and a recent *in vivo* measurement (Lee *et al*., 2015) at the apex of a mouse cochlea, when excited at 80 dB SPL.

The tapered model of the mouse cochlea shows a better match in amplitude compared with the human case, although the measured phase shows a greater lag. It is interesting to see that the tapering in the mouse model does not play a significant effect, as the uniform model does not manifest as much difference, less than 3 dB, as the human case. We suspect that this less discrepancy of amplitude between the tapered and uniform models is due to the fact that the mouse cochlea has the least variation among the selected species, as seen in Fig. 2 and Fig. 3.

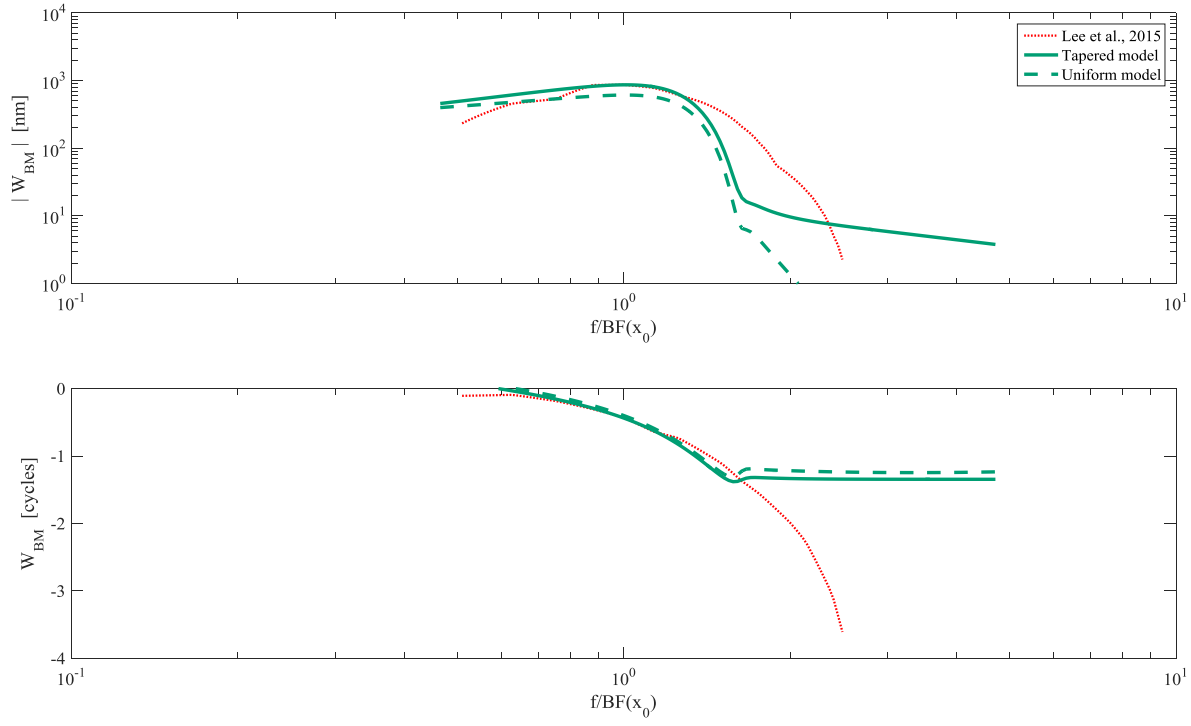

FIG. 9. (color online) The frequency response of the BM displacement magnitude and phase along the linearly tapered and uniform mouse cochlear models with a Q factor of 2.5, together with experimental measurements (Lee *et al.*, 2015) with 80 dB SPL. Frequencies are normalized by the best frequency, BF(x_0) ≈ 3.2 kHz, at this level.

VI. CONCLUSIONS

As an improvement and extension to the previous work, a modification of the widely used uniform box model is developed here with a linear variation of fluid chamber cross-sectional areas and the basilar membrane width, which both play an important role in the BM passive response. Discrete formulations for the far-field fluid coupling are derived, which are suitable for both uniform and tapered cochlea box models. Although a linear approximation is not

accurate enough to represent the entire geometrical features in the cochleae, especially at the basal region where the anatomy is more complicated, it is found that this approximation is not bad when reproduces the passive cochlear response measured at a certain distance away from the base. It is also interesting to see that the selected species all show an approximately linear variation when the square root of the effective area is considered.

The BM velocity calculated using the linearly tapered model is greater than that using the uniform models and the difference in BM velocity peak is frequency-dependent, e.g. the difference is about 20 dB at 5000 Hz but about 5 dB at 500 Hz. This is because that the ratio of the BM width to the fluid chamber width, B/W, increases with position in the tapered model, which leads to a decrease in the BM response. The tapered model has a smaller effective area and greater B/W at the apical end but still provides higher BM response than the uniform model with average parameters, which suggests that the tapering helps to maintain efficiency in the transfer of acoustic energy to the cochlea at low frequencies, as suggested by Shera and Zweig (1991). The other difference between the tapered and uniform models is that the best position, where the BM response is maximal, is different even these models have the same BM admittance. Close to the base, the tapered model has smaller fluid added mass, which shifts its best position towards the apex. Whereas close to the apical region, this fluid added mass of the linearly tapered model becomes greater than that of the uniform models, thus shifts its best position towards the base.

The dissipative effect is accounted for here by a damping term in the BM admittance only, but this does not seem to be sufficient for an accurate phase response. The mouse models show a slower phase drop compared with the experiment after the best frequency. The phase response could be better if a greater Q factor was used in the micromechanical model, Q=5 for example, but this leads to a worse fit for the amplitude. This is contradictory since one would expect that a broad and smooth amplitude would need a small Q factor, high damping,

whereas a fast phase drop would need a large Q factor, low damping. We suspect that a combination of fluid viscosity (Wang *et al*., 2016) and BM damping may improve model prediction.

An important advantage of this approach is that it provides a general way to calculate the fluid coupling even when the fluid chambers are non-uniform. By combining the fluid coupling with the basilar membrane dynamics, the coupled response of the cochlea can be readily calculated with low computational efforts.

ACKNOWLEDGMENT

The authors declare no existing or potential conflict of interest. Guangjian Ni is supported by grants from EPSRC (Engineering nonlinearity, Grant No. EP/K003836/1) and MRC (Interaction between sensory and supporting cells in the organ of Corti: basis for sensitivity and frequency selectivity of mammalian cochlea, Grant No. MR/N004299/1).

REFERENCE

Cabezudo, L. M. (**1978**). "The ultrastructure of the basilar membrane in the cat," Acta Oto-Laryngol. **86**, 160–175.

Cai, H., Manoussaki, D., and Chadwick, R. S. (**2005**). "Effects of coiling on the micromechanics of the mammalian cochlea," J. R. Soc. Interface **2**, 341–348.

Dallos, P. (**1970**). "Low-frequency auditory characteristics: Species dependence," J. Acoust. Soc. Am. **48**, 489–499.

de Boer, E. (**1981**). "Short waves in three-dimensional cochlea models: Solution for a 'block' model," Hear. Res. **4**, 53-77.

de Boer, E., and Viergever, M. A. (**1982**). "Validity of the Liouville-Green (or WKB) method for cochlear mechanics," Hear. Res. **8**, 131–155.

de Boer, E. (**1984**). "Auditory physics. Physical principles in hearing theory. II," Phys. Rep. **105**, 141–226.

de Boer, E. (**1991**). "Auditory physics. Physical principles in hearing theory. III.," Phys. Rep. **203**, 125–231.

de Boer, E. (**1996**). "Mechanics of the cochlea: Modelling efforts," in *The cochlea*, edited by Dallos, P., Popper, A. N., and Fay, R. R. (Springer, New York), pp. 258–317.

de La Rochefoucauld, O., and Olson, E. S. (**2007**). "The role of organ of corti mass in passive cochlear tuning," Biophys. J. **93**, 3434–3450.

Elliott, S. J., Lineton, B., and Ni, G. (**2011**). "Fluid coupling in a discrete model of cochlear mechanics," J. Acoust. Soc. Am. **130**, 1441–1451.

Elliott, S. J., Ni, G., Mace, B. R., and Lineton, B. (**2013**). "A wave finite element analysis of the passive cochlea," J. Acoust. Soc. Am. **133**, 1535–1545.

Fahy, F., and Gardonio, P. (**2007**). *Sound and structural vibration: Radiation, transmission and response* (Elsevier Academic Press, Oxford, UK), pp. 449–519.

Fernández, C. (**1952**). "Dimensions of the Cochlea (Guinea Pig)," J. Acoust. Soc. Am. **24**, 519–523.

Fletcher, N. H., and Rossing, T. D. (**2008**). *The physics of musical instruments* (Springer, New York), pp. 207.

Greenwood, D. D. (**1990**). "A cochlear position-frequency function for several species – 29 years later," J. Acoust. Soc. Am. **87**, 2592–2605.

Gundersen, T., Skarstein, O., and Sikkeland, T. (**1978**). "A study of the vibration of the basilar membrane in human temporal bone preparations by the use of the Mossbauer effect," Acta Oto-Laryngol. **86**, 225–232.

Keiler, S., and Richter, C. P. (**2001**). "Cochlear dimensions obtained in hemicochleae of four different strains of mice: CBA/CaJ, 129/CD1, 129/SvEv and C57BL/6J," Hear. Res. **162**, 91–104.

Kim, N., Homma, K., and Puria, S. (**2011**). "Inertial bone conduction: symmetric and anti-symmetric components," JARO 12, 261–279.

Lee, H. Y., Raphael, P. D., Park, J., Ellerbee, A. K., Applegate, B. E., and Oghalai, J. S. (**2015**). "Noninvasive in vivo imaging reveals differences between tectorial membrane and basilar membrane traveling waves in the mouse cochlea," Proc. Natl. Acad. Sci. U. S. A. **112**, 3128–3133.

Lesser, M. B., and Berkley, D. A. (**1972**). "Fluid mechanics of the cochlea. Part I.," J. Fluid. Mech. **51**, 497–512.

Liberman, M. C. (**1982**). "The cochlear frequency map for the cat: labeling auditory-nerve fibers of known characteristic frequency," J. Acoust. Soc. Am. **72**, 1441–1449.

Loh, C . H. (**1983**). "Multiple scale analysis of the spirally coiled cochlea," J. Acoust. Soc. Am. **74**, 95-103.

Manoussaki, D., and Chadwick, R. S. (**2000**). "Effects of geometry on fluid loading in a coiled cochlea," SIAM J. Appl. Math. **61**, 369–386.

Neely, S. T. (**1981**). "Finite difference solution of a two-dimensional mathematical model of the cochlea," J. Acoust. Soc. Am. **69**, 1386-1393.

Neely, S. T. (**1985**). "Mathematical modelling of cochlear mechanics," J. Acoust. Soc. Am. **78**, 345–352.

Ni, G., Elliott, S. J., Lineton, B., and Saba, R. (**2011**). "Finite element modelling of fluid coupling in the coiled cochlea," in *What Fire is in Mine Ears: Progress in Auditory Biomechanics*, edited by C. A. Shera, and E. S. Olson, pp. 350-355.

Ni, G., and Elliott, S. J. (**2013**). "Effect of basilar membrane radial velocity profile on fluid coupling in the cochlea," J. Acoust. Soc. Am. **133**, EL181–EL187.

Ni, G., and Elliott, S. J. (**2015**). "Comparing methods of modeling near field fluid coupling in the cochlea," J. Acoust. Soc. Am. **137**, 1309–1317.

Parthasarathi, A. A., Grosh, K., and Nuttall, A. L. (**2000**). "Three-dimensional numerical modeling for global cochlear dynamics," J. Acoust. Soc. Am. **107**, 474–485.

Peterson, L. C., and Bogert, B. P. (**1950**). "A dynamical theory of the cochlea," J. Acoust. Soc. Am. **22**, 369–381.

Ranke, O. F. (**1950**). "Theory of Operation of the Cochlea: A Contribution to the Hydrodynamics of the Cochlea," J. Acoust. Soc. Am. **22**, 772–777.

Puria, S., and Allen, J. B. (**1991**). "A parametric study of cochlear input impedance," J. Acoust. Soc. Am. **89**, 287-309.

Ranke, O. F. (1950). "Theory of Operation of the Cochlea: A Contribution to the Hydrodynamics of the Cochlea," J. Acoust. Soc. Am. **22**, 772-777.

Rau, C., Hwang, M., Lee, W. K., and Richter, C. P. (**2012**). "Quantitative X-ray Tomography of the Mouse Cochlea," PloS one **7**, e33568.

Robles, L., and Ruggero, M. A. (**2001**). "Mechanics of the Mammalian Cochlea," Physiol. Rev. **81**, 1305–1352.

Shera, C. A., and Zweig, G. (**1991**). "A symmetry suppresses the cochlear catastrophe," J. Acoust. Soc. Am. **89**, 1276-1289.

Shera, C. A., Tubis, A., and Talmadge, C. L. (**2004**). "Do forward- and backward-traveling waves occur within the cochlea? Countering the critique of Nobili et al.," JARO **5**, 349-359.

Shera, C. A. (**2007**). "Laser amplification with a twist: Traveling-wave propagation and gain functions from throughout the cochlea," J. Acoust. Soc. Am. **122**, 2738–2758.

Siebert, W. M. (**1974**). "Ranke revisited---a simple short-wave cochlear model," J. Acoust. Soc. Am. **56**, 594–600.

Sondhi, M. M. (**1978**). "Method for computing motion in a two-dimensional cochlear model," J. Acoust. Soc. Am. **63**, 1468–1477.

Steele, C. R., and Taber, L. A. (**1979a**). "Comparison of WKB and finite difference calculations for a two-dimensional cochlear model," J. Acoust. Soc. Am. **65**, 1001–1006.

Steele, C. R., and Taber, L. A. (**1979b**). "Comparison of WKB calculations and experimental results for three-dimensional cochlear models," J. Acoust. Soc. Am. **65**, 1007–1018.

Steele, C. R., and Taber, L. A. (**1981**). "Three-dimensional model calculations for guinea pig cochlea," J. Acoust. Soc. Am. **69**, 1107–1111.

Steele, C.R., and Zais, J. G. (**1985**). "Effect of coiling in a cochlear model," J. Acoust. Soc. Am. **77**, 1849–1852.

Stenfelt, S., Puria, S., Hato, N., and Goode, R. L. (**2003**). "Basilar membrane and osseous spiral lamina motion in human cadavers with air and bone conduction stimuli," Hear. Res. **181**, 131–143.

Thorne, M., Salt, A. N., DeMott, J. E., Henson, M. M., Henson, O. W., Jr., and Gewalt, S. L. (**1999**). "Cochlear fluid space dimensions for six species derived from reconstructions of three-dimensional magnetic resonance images," Laryngoscope **109**, 1661–1668.

Viergever, M. A. (1978). "Basilar membrane motion in a spiral-shaped cochlea," J. Acoust. Soc. Am. **64**, 1048-1053.

Viergever, M. A. (**1980**). *Mechanics of the Inner Ear-a Mathematical Approach*, PhD thesis (Delft University of Technology, Netherland), p. 174.

Vetesn ḱ, A., and Nobili, R. (**2006**). "The approximate scaling law of the cochlea box model," Hear. Res. **222**, 43–53.

Wang, Y., Steele, C. R., and Puria, S. (**2016**). "Cochlear Outer-Hair-Cell Power Generation and Viscous Fluid Loss," Sci Rep **6**, 19475.

Watts, L. (**2000**). "The mode-coupling Liouville-Green approximation for a two-dimensional cochlear model," J. Acoust. Soc. Am. **108**, 2266–2271.

Wever, E. G., (1949). *Theory of Hearing* (Wiley, New York), pp. 484.

Wittbrodt, M. J., Steele, C. R., and Puria, S. (**2006**). "Developing a Physical Model of the Human Cochlea Using Microfabrication Methods," Audiol. Neuro-Otol. **11**, 104–112.

Zweig, G. (**1976**). "Basilar membrane motion," Cold Spring Harbor symposia on quantitative biology **40**, 619–633.

Zwislocki, J. J. (**1953**). "Review of recent mathematical theories of cochlear dynamics," J. Acoust. Soc. Am. **25**, 743–751.